Coupling between a finite element model of coronary artery mechanics and a microscale agent-based model of smooth muscle cells through trilinear interpolation.

Fotin Aleksei[1][0000−0003−4127−6209] and Zun Pavel[1][0000−0001−6176−1143]

ITMO University, Russia
alexseixiv@gmail.com

Abstract. Finite element (FE) simulation is an established approach to mechanical simulation of angioplasty and stent deployment. Agent-based (AB) models are an alternative approach to biological tissue modeling in which individual cells can be represented as agents and are suitable for studying biological responses. By combining these two approaches, it is possible to leverage the strengths of each to improve the in silico description of angioplasty or stenting and the following healing response. Here we propose a couping between FE and AB vascular tissue models using trilinear interpolation, where the stresses (and strains) in the AB model arise directly from the forces of interaction between individual agents. The stress values for FE and AB models are calculated and compared.

Keywords: arterial tissue · mechanical model · agent-based model · finite-element model.

1 Introduction

Finite element simulation is now often used to study stent implantation in coronary arteries *in silico*. Using finite element method (FEM) reproduces the mechanical behavior on the continuous scale of the stent, balloon, and artery. On the other hand, an approach that allows to explore the scale of cellular interaction is offered by agent-based models (ABM) [1]. Although the FEM [2–4] and ABM [5–7] approaches could be used independently to study both the mechanical processes during stenting and the biological response after stent deployment, nevertheless, combining the two methods will provide a more accurate and reliable approach to analysis both from the mechanical point of view (through FEM) and from the biological point of view (through ABM).

The strength of FE modelling lies in the ability to accurately simulate large-scale mechanical behaviour. Cell-resolved AB models, on the other hand, can naturally include cell-scale biological behaviour [6]. Most of the AB models proposed so far are center-based (CB) models, meaning that each cell is approximated as a sphere, and the forces act between cell centers, e.g. [6, 8–11], which

allow for simulations on the order of several millions of cells, but simplify the microscopic properties. Deformable cell (DC) models present an alternative approach. They produce a much more detailed microscopic behaviour, but also have much higher computational costs per cell, e.g. [12, 13].

Here, a method is proposed to combine the two approaches to analyze stent deployment in coronary arteries. The purpose of this paper is to propose a method for integrating the results of finite element modeling of stent deployment into an agent-based model, which, in turn, will be used to study tissue growth and vessel restenosis. Thus, we want to obtain an equivalent mechanical response for the agent-based model based on the results of the finite element simulation, which is important for obtaining reliable predictions of the development of restenosis.

One-way couplings of FE and AB models for vascular walls have been proposed before, e.g. in [14–16], as well as a two-way coupling approach [17]. Note that in all these papers the agents are uniformly seeded on the deformed post-deployment vessel, do not interact mechanically, and the stress value is passed to them as an external parameter. Here we propose an alternative approach where the stress (and strain) in the AB model are computed directly from the interaction forces between individual agents.

2   Methods

This section introduces the AB and FE models used in this study, the coupling method, and outlines the computational experiments performed.

2.1   Finite element model

The geometric model of an idealized artery represented as a straight cylindrical tube was discretized with linear hexahedral elements with reduced integration (C3D8R). For simplicity, the wall of the vessel consists only of the tunica media, the middle layer of the artery. The reason is that tunica media is responsible for a large part of the vessel's mechanical behaviour, and also its mechanical properties are relatively less varied between individuals. A material model with hyperelastic behavior was calibrated to replicate the experimental stress-strain relationships reported in [18]. In particular, the model parameters were selected to reproduce the circumferential behavior, since it is the prevalent strain direction in the vessel during the pressurization and stenting procedure. Simulation of vessel pressurization was performed by imposing an increase in pressure on the lumen surface until the desired value ($100 \ mmHg$) was reached.

All finite element analyses were performed using Abaqus/Explicit (SIMULIA Corp., USA), and each was checked to work in the quasi-static regime.

2.2   Agent-based model

The model presented here uses a design similar to the models presented in [5, 6, 19]. It is a center-based AB model, where each cell is represented as an elastic

sphere, which can interact with its neighbours via elastic repulsion and pairwise bond forces. The elastic repulsion force pushes overlapping agents away, while the bonds are established for all initially neighbouring cells and are used to simulate tissue's tensile properties, which *in vivo* are provided by cell-cell adhesion as well as by extracellular molecules such as collagen and elastin [20]. Both the elastic and the bond forces in the model act between the cell centers.

For elastic repulsion, a Neo-Hookean extension of Hertz elastic sphere contact is used as described in [5, 19]:

$$F_{hertz} = \frac{8a^3 B(16a^2 - 36\pi aR + 27\pi^2 R^2)}{3R(4a - 3\pi R)^2} \tag{1}$$

where R is the effective radius calculated as

$$R = \frac{R_1 R_2}{R_1 + R_2}$$

and a is the contact area and is approximated as

$$a = \sqrt{R \cdot (R_1 + R_2 - d)}$$

Here, R_1 and R_2 are the agents' radii, d is the distance between their centres, B is the elastic constant. For all experiments, the elastic constant was set to $B = 0.2\ MPa$ based on [5].

The attractive bond force is based on several different mechanisms (cell adhesion and extracellular fibers) and its purpose in the model is to provide a realistic macroscopic behaviour. We opt to use a polynomial attractive force which is fitted to mimic the macroscopic behaviour of the FE model and the experimental data. The force between neighbouring cells is calculated by the following formula:

$$F_{bond} = (R_1 + R_2)^2 \cdot \sum_{k=1}^{N} c_k \sigma^k, \quad \sigma > 0 \tag{2}$$

where the bond strain σ equals

$$\sigma = \frac{d - R_1 - R_2}{R_1 + R_2}$$

All c_k coefficients were restricted to non-negative values, to ensure that the energy minimum for each bond is located at zero strain. Following the FE model, we use 6th order polynomials for the bond forces ($N = 6$). Separate sets of coefficients $c_1..c_6$ are used for intima, media and adventitia in the three-layer wall model considered here.

The cells are placed randomly while maintaining a minimal distance between each pair of cells. For this, we use a three-dimensional Poisson disc sampling generated by Bridson's algorithm [21]. This sampling allows us to produce isotropic tissue with an almost constant density. A sample of the generated tissue is shown in figure 1. Each cell was assigned the same radius $r = 0.015\ mm$.

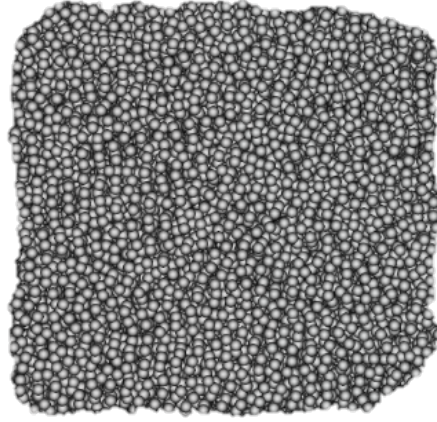**Fig. 1.** Isotropic tissue sample generated by a 3D Poisson Disc sampling.

The AB model is implemented as a part of the ISR3D model[1].

2.3 Coupling AB and FE simulations

For inflation and stenting simulations, AB vessels were generated based on FE geometries. For each finite element in the arterial wall and in the stent, agents were placed inside using Poisson Disc (PD) sampling. For each agent, bonds were added to agents within a cutoff distance. The tissue was then equilibrated to improve the structure at the interfaces between different finite elements, reducing gaps and overlaps of agents.

To verify the equivalence between the finite element model and the agent-based model, the displacement history recorded with the finite element simulation was imposed on the AB model, and the lumen inner diameter-pressure relation was observed. The correspondence of this relationship obtained with the finite element method and with the agent-based model allows to affirm that the two models are equivalent.

The displacement is imposed by recording the trajectories for all nodes in the FE artery. Then, for each agent, its trajectory is calculated using trilinear interpolation. This method is an extension of linear and bilinear interpolation for the 3D case. In essence, the method is a sevenfold application of linear interpolation according to the formula:

$$c = c_0 + \frac{dist(\tilde{c}, \tilde{c_0})}{dist(\tilde{c_1}, \tilde{c_0})}(c_1 - c_0) \tag{3}$$

where $\tilde{c_i}$ is the coordinate of the point i, c_i is the known offset at the point i, c is the result of the interpolation.

---

[1] https://github.com/ISR3D/ISR3D

Thus, for each agent, it is necessary to determine the nodes and the offset of the finite element in which the agent is located, and sequentially calculate the coefficients c_{00}, c_{01}, c_{10}, c_{11}, c_0, c_1, c (Fig. 2).The last coefficient is the required trajectory for agent.
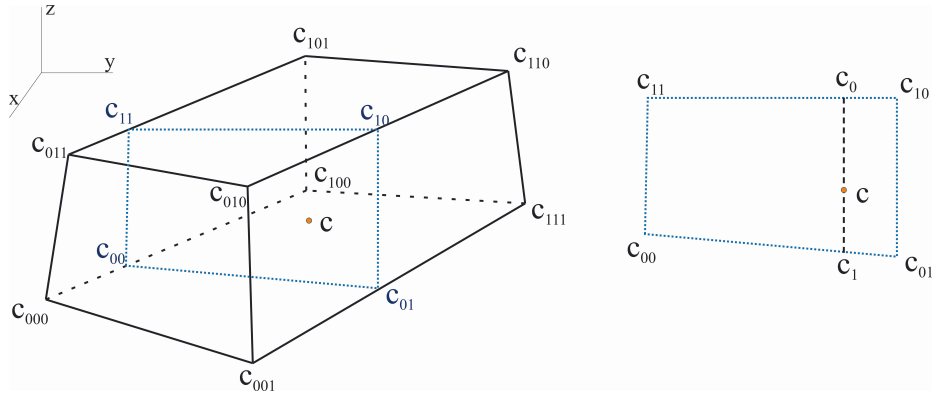

Fig. 2. Trilinear interpolation for point c in cuboid.

During the displacement, the agents in the vessel wall interact via the forces described above, providing stress-strain dynamics for the deployment. After the agents reach the end of their trajectories, the lumen surface is fixed in place, and the rest of the agents are equilibrated.

2.4   Pressurization tests

Pressurization tests were performed in a simple cylindrical vessel (length $4.5\ mm$, inner radius $1.26\ mm$, outer radius $2.32\ mm$). The FE vessel was generated first (Fig. 3), and then the AB vessel (containing 1767269 agents, Fig. 4) was generated. Variant of this vessel was considered where the cylinder is made entirely of the media tissue. Pressurization to $100\ mmHg$ ($13.332\ kPa$) was simulated with the FE model, followed by the AB model, coupled as described before. Pressurization was considered: one, where no specific boundary conditions were imposed on the nodes at the ends of the vessel; the other, where the nodes (FE) or agents (AB) on both ends of the vessel were blocked from moving along the longitudinal direction.

2.5   Assessing the results

The values of inner radius change and intramural stress were used for comparison between AB and FE. The stress was considered in three directions relative to the vessel axis: circumferential, radial, and axial. The intramural stress for the FE model was calculated from the per-element stress matrix. In AB model, the
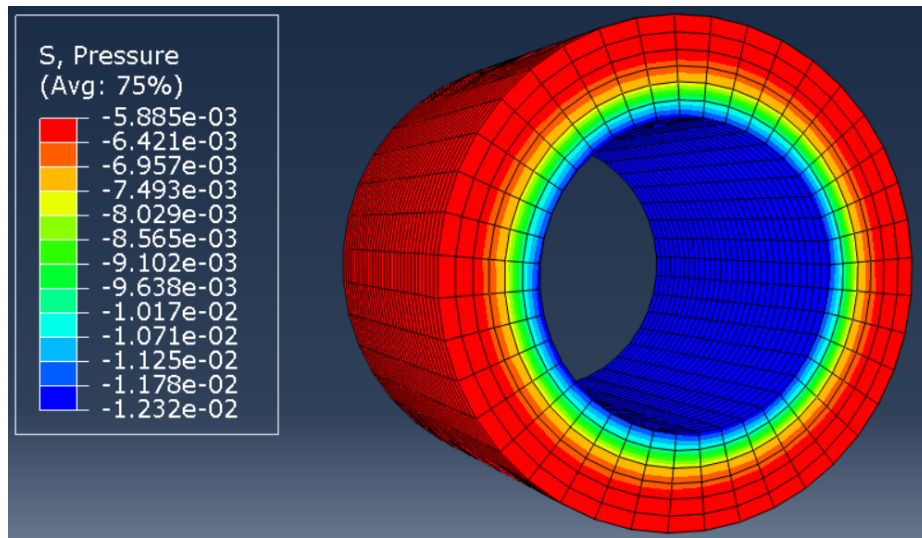
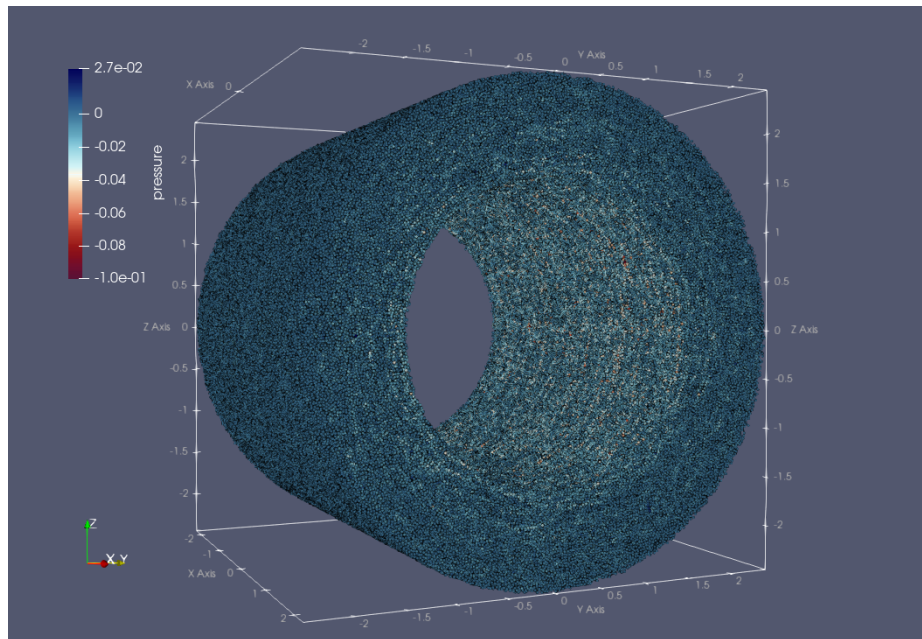**Fig. 3.** Results of the finite element model of the vessel.

Fig. 4. The agent-based vessel generated from the finite element model after pressurization displacement.

stress was calculated as an instantaneous local virial stress [1, 22], calculated from pairwise interaction forces and agent size. The virial stress for i-th agent along m-th coordinate is calculated as:

$$\tau_m^i = \frac{3}{4\pi R_i^3} \sum_{j \in neighbours} f_{ij}^m \cdot (R_i + \frac{d_{ij} - R_i - R_j}{2}), \ m \in \{x, y, z\} \qquad (4)$$

where j is an index that goes over all neighbouring agents interacting with the i-th agent, and f_{ij}^m. is the force exerted by j-th on i-th agent along m-th coordinate. The AB pressure then is calculated as

$$p_{virial} = -\frac{\tau_x^i + \tau_y^i + \tau_z^i}{3} \qquad (5)$$

To enable comparison of stresses on the same scale, and to smooth out the local fluctuations in the virial stress that arise from the inhomogeneities in the AB tissue, we allocate the stress values from both FE and AB simulations to bins and average the values inside them. This results in heatmaps of stresses for each case.

Since the vessels are cylindrically symmetric, we choose to allocate the bins based on the longitudinal coordinate x and the radial distance r; all the points around the vessel circumference with the same x and r end up in the same bin. The bin dimensions are 0.32 mm both for x and r directions. Fig. 5 shows a schematic illustration of this approach.
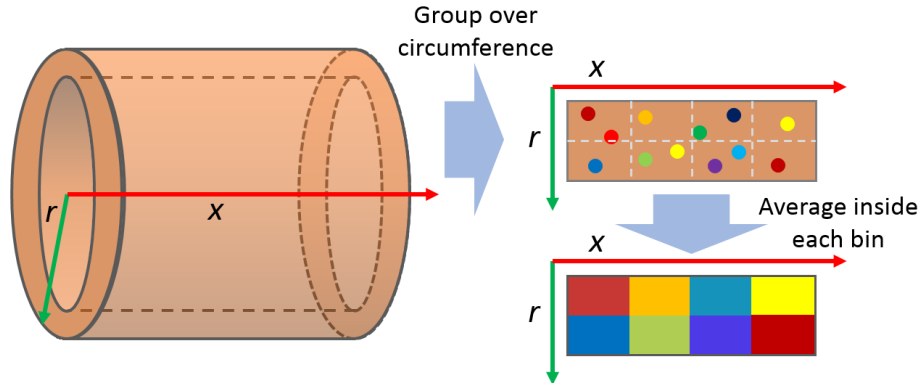

Fig. 5. A schematic depiction of the averaging using bins in the rx plane. First, the points are grouped over the circumferential direction. Then, the value of each bin is calculated as the average of all points in it.

The results are analyzed with NumPy[2] and Pandas[3], and the plots are generated with Matplotlib[4] and Seaborn[5]. 3D results from the AB model are plotted with Paraview[6].

3   Results

To compare FE and AB models, we performed pressurization tests at a pressure of 100 $mmHg$. For the case of a segment of media with free ends, a cross-sectional distribution of intramural pressure for the FE and AB vessels is shown in the figure 6 and in the table 3 . The case of a segment of media with fixed ends is shown in the figure 7 and in the table 3.
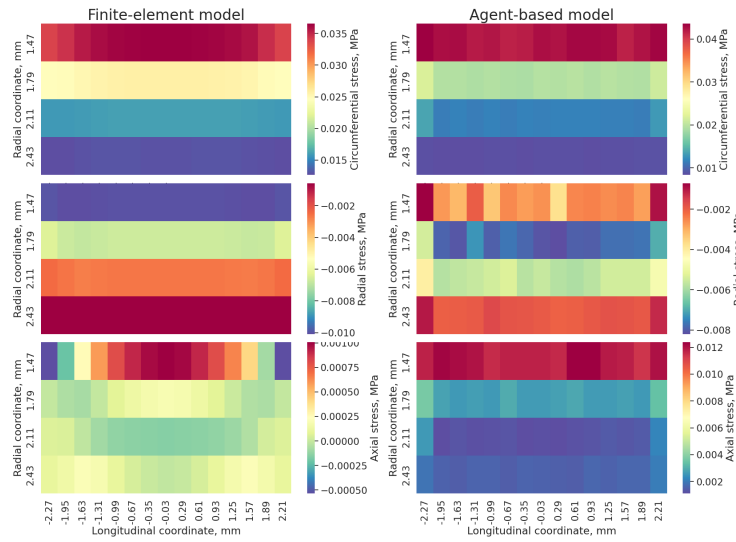

Fig. 6. Average intramural stress distribution (MPa) for AB and FE models for inflation at 100 mmHg. Media tissue, unconstrained ends. Top: circumferential, middle: radial, bottom: axial stress. Note that the scales are different for each subplot.

The inner radius of the AB model vessel has been increased from 1.26 mm to 1.47 mm, the same as the FE vessel. As for the outer radius, for the agent-based model it changed from 2.32 mm to 2.45 mm, and in the finite element simulation from 2.32 mm to 2.43 mm.

---

[2] https://numpy.org

[3] https://pandas.pydata.org

[4] https://matplotlib.org

[5] https://seaborn.pydata.org
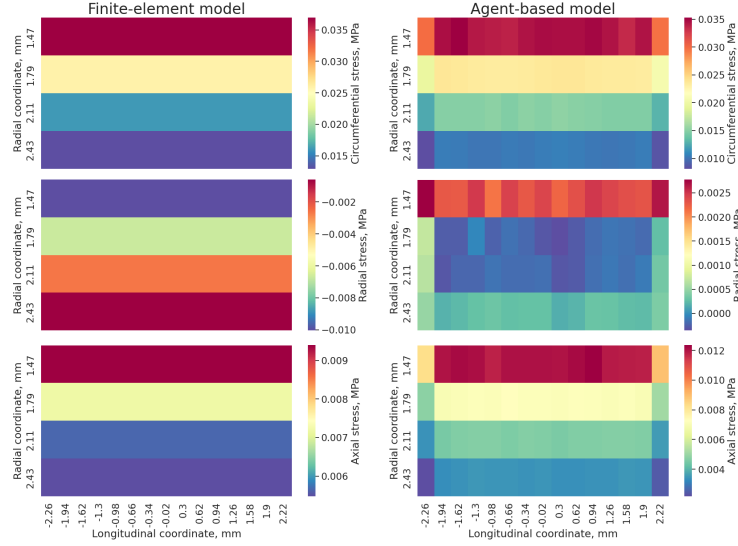
[6] https://www.paraview.org

Fig. 7. Average intramural stress distribution (MPa) for AB and FE models for inflation at 100 mmHg. Media tissue, ends constrained to the cross-sectional plane. Top: circumferential, middle: radial, bottom: axial stress. Note that the scales are different for each subplot.

Table 1. Intramural stress distribution (MPa) for AB and FE models for inflation at 100 mmHg. Media tissue, ends constrained to the cross-sectional plane.

	mean, FE	mean, AB	average inaccuracy
Circumferential stress	0,0229 MPa	0,0203 MPa	12,80%
Radial stress	-0,0049 MPa	0,0006 MPa	116,10%
Axial stress	0,0069 MPa	0,0065 MPa	23,00%

Table 2. Intramural stress distribution (MPa) for AB and FE models for inflation at 100 mmHg. Media tissue, unconstrained ends.

	mean, FE	mean, AB	average inaccuracy
Circumferential stress	0,0225 MPa	0,0206 MPa	25,40%
Radial stress	-0,0049 MPa	-0,0043 MPa	100,30%
Axial stress	0,0001 MPa	0,0044 MPa	6764,60%

4   Discussion

The inflation tests for a cylindrical segment of the vessel demonstrate a good agreement between AB and FE for the final inner and outer radii of the vessel. The inner radius in AB is exactly the same as FE, and the outer radius is slightly higher. The likely cause is that incompressibility is not enforced in any way in the AB model, unlike FE. Even if individual agents stay at the same equilibrium distance from each other, the enveloping volume may differ. There are ways to enforce a constant volume in particle-based methods: for example, [23, 24] describe such a method for smooth particle hydrodynamics (SPH). However, testing these methods is outside the scope of this article.

The agreement between the two considered models is good in terms of circumferential stress (the average deviation is no more than 25%), and somewhat weaker for the radial and axial stress components. It should be noted that the circumferential stress is the largest in the pressurization scenario consivered here and also in clinically relevant stenting scenarios, and is considered the most important for the biological response. A possible reason for the discrepancy in the axial and the circumferential components, in addition to the compressibility of AB tissue, is one limitation intrinsic to center-based AB models: since the cells cannot change their shape, virial stress calculations are known to be inaccurate, especially for compressive behaviour [1]. The only way to avoid this is by using deformable cell models [12], which are a lot more expensive computationally.

5   Conclusions

The pressurization tests show that the presented AB model is in a good match with the geometry of the FE model. This allows the AB model to capture deformation-based cues, important for the cells' biological response.

The averaged stress in the tissue is also close between the two models. However, there are noticeable fluctuations on the scale of individual cells.

This means that the coupling mechanism considered in this article can be used to directly impose mechanical strains and stresses from finite element models onto agent-based biological models, to inform the biological response to mechanical cues in tissue simulations. However, stresses should be used more cautiously than strains, since the difference between FE and AB is larger, although it is comparable with biological variability between individual vessels [18].

6   Acknowledgements

References

1. Van Liedekerke, P., Palm, M.M., Jagiella, N. et al. Simulating tissue mechanics with agent-based models: concepts, perspectives and some novel results. Comp. Part. Mech. **2**, 401-444 (2015). https://doi.org/10.1007/s40571-015-0082-3

2. Morlacchi, S., Pennati, G., Petrini, L., et al. Influence of plaque calcifications on coronary stent fracture: A numerical fatigue life analysis including cardiac wall movement. J Biomech. **47**, 899-907 (2014). https://doi.org/10.1016/j.jbiomech.2014.01.007

3. Escuer Javier, Martínez Miguel A., McGinty Sean & Peña Estefanía. Mathematical modelling of the restenosis process after stent implantation. J. R. Soc. Interface. **16**, (2019). https://doi.org/10.1098/rsif.2019.0313

4. Gierig, M., Wriggers, P. & Marino, M. Computational model of damage-induced growth in soft biological tissues considering the mechanobiology of healing. Biomech Model Mechanobiol **20**, 1297–1315 (2021). https://doi.org/10.1007/s10237-021-01445-5

5. Melnikova, N., Svitenkov, A., Hose, D. & Hoekstra, A. A cell-based mechanical model of coronary artery tunica media. J. R. Soc. Interface **14**, (2017). https://doi.org/10.1098/rsif.2017.0028

6. Zun, P.S., Narracott, A.J., Chiastra, C. et al. Location-Specific Comparison Between a 3D In-Stent Restenosis Model and Micro-CT and Histology Data from Porcine In Vivo Experiments. Cardiovasc Eng Tech **10**, 568-582 (2019). https://doi.org/10.1007/s13239-019-00431-4

7. Corti, A., Chiastra, C., Colombo, M., Garbey, M., Migliavacca, F. & Casarin, S. A fully coupled computational fluid dynamics – agent-based model of atherosclerotic plaque development: Multiscale modeling framework and parameter sensitivity analysis. Computers In Biology And Medicine **118**, (2020). https://doi.org/10.1016/j.compbiomed.2020.103623

8. Walker, D., Georgopoulos, N. & Southgate, J. Anti-social cells: Predicting the influence of E-cadherin loss on the growth of epithelial cell populations. Journal Of Theoretical Biology. **262**, 425-440 (2010). https://doi.org/10.1016/j.jtbi.2009.10.002

9. Schlüter, D., Ramis-Conde, I. & Chaplain, M. Multi-scale modelling of the dynamics of cell colonies: insights into cell-adhesion forces and cancer invasion from in silico simulations.. Journal Of The Royal Society, Interface / The Royal Society. **12** pp. 20141080- (2015). https://doi.org/10.1098/rsif.2014.1080

10. Ingham-Dempster, T., Walker, D. & Corfe, B. An agent-based model of anoikis in the colon crypt displays novel emergent behaviour consistent with biological observations. Royal Society Open Science. **4** (2017). https://doi.org/10.1098/rsos.160858

11. Tahir, H., Hoekstra, A., Lorenz, E., Lawford, P., Hose, D., Gunn, J. & Evans, D. Multi-scale simulations of the dynamics of in-stent restenosis: impact of stent deployment and design. Interface Focus. **1**, 365-373 (2011). https://doi.org/10.1098/rsfs.2010.0024

12. Van Liedekerke, P., Neitsch, J., Johann, T., Warmt, E., Gonzàlez-Valverde, I., Hoehme, S., Grosser, S., Kaes, J. & Drasdo, D. A quantitative high-resolution computational mechanics cell model for growing and regenerating tissues. Biomechanics And Modeling In Mechanobiology **19**, 189-220 (2019). https://doi.org/10.1007/s10237-019-01204-7

13. Dabagh, M., Jalali, P., Butler, P., Randles, A. & Tarbell, J. Mechanotransmission in endothelial cells subjected to oscillatory and multi-directional shear flow. Journal Of The Royal Society Interface. **14** (2017). https://doi.org/10.1098/rsif.2017.0185

14. Keshavarzian, M., Meyer, C. & Hayenga, H. Mechanobiological model of arterial growth and remodeling. Biomechanics And Modeling In Mechanobiology. **17**, 87-101 (2018,2). https://doi.org/10.1007/s10237-017-0946-y

15. Nolan, D. & Lally, C. An investigation of damage mechanisms in mechanobiological models of in-stent restenosis. Journal Of Computational Science. **24** pp. 132-142 (2018). https://doi.org/10.1016/j.jocs.2017.04.009

16. Boyle, C., Lennon, A. & Prendergast, P. Application of a mechanobiological simulation technique to stents used clinically. Journal Of Biomechanics. **46**, 918-924 (2013). https://doi.org/10.1016/j.jbiomech.2012.12.014

17. Li, S., Lei, L., Hu, Y., Zhang, Y., Zhao, S. & Zhang, J. A fully coupled framework for in silico investigation of in-stent restenosis. Computer Methods In Biomechanics And Biomedical Engineering. **22**, 217-228 (2019). https://doi.org/10.1080/10255842.2018.1545017

18. Holzapfel, G., Sommer, G., Gasser, C. & Regitnig, P. Determination of layer-specific mechanical properties of human coronary arteries with nonatherosclerotic intimal thickening and related constitutive modeling. American Journal Of Physiology-Heart And Circulatory Physiology **289**, 2048-2058 (2005). https://doi.org/10.1152/ajpheart.00934.2004

19. Zun, P., Anikina, T., Svitenkov, A. & Hoekstra, A. A comparison of fully-coupled 3D in-stent restenosis simulations to In-vivo Data. Frontiers In Physiology **8**, 284 (2017). https://doi.org/10.3389/fphys.2017.00284

20. Ratz, P. Mechanics of Vascular Smooth Muscle. In Comprehensive Physiology, R. Terjung (Ed.) **2**, 111-168 (2015). https://doi.org/10.1002/cphy.c140072

21. Bridson, Robert. Fast Poisson disk sampling in arbitrary dimensions. In ACM SIGGRAPH 2007 sketches (SIGGRAPH '07). Association for Computing Machinery, New York, NY, USA, 22–es (2007). https://doi.org/10.1145/1278780.1278807

22. Subramaniyan, A. & Sun, C. Continuum interpretation of virial stress in molecular simulations. International Journal Of Solids And Structures **45**, 4340-4346 (2008). https://doi.org/10.1016/j.ijsolstr.2008.03.016

23. Bender, J. & Koschier, D. Divergence-free smoothed particle hydrodynamics. Proceedings of the 14th ACM SIGGRAPH / Eurographics Symposium on Computer Animation, 147-155 (2015). https://doi.org/10.1145/2786784.2786796

24. Bender, J. & Koschier, D. Divergence-Free SPH for Incompressible and Viscous Fluids. IEEE Transactions On Visualization And Computer Graphics **23**, 1193-1206 (2017). https://doi.org/10.1109/TVCG.2016.2578335